MTLA 30 (2023) 101859

Contents lists available at ScienceDirect

Materialia

journal homepage: www.elsevier.com/locate/mtla

Full Length Article

Dextrin hydrogel loaded with a macroporous Bonelike® scaffold and dental pulp stem cells for critical-sized defect repair

Alexandra Machado [a,b], Isabel Pereira [a], José Eduardo Pereira [c,d,e], Luís Maltez [c,d,e], Ana Brandão [f], Rui Alvites [d,g,h], Ana Catarina Sousa [d,g,h], Mariana Branquinho [d,g,h], Ana Rita Caseiro [d,h,i,j], Sílvia Santos Pedrosa [d,g,h,k], Ana Colette Maurício [d,g,h], Isabel Pires [c,d,e], Justina Prada [c,d,e], José Domingos Santos [l], Miguel Gama [a,b,*]

[a] Centre of Biological Engineering (CEB), University of Minho, 4710-057 Braga, Portugal
[b] Associate Laboratory (LABBELS), Braga, Guimarães, Portugal
[c] Animal and Veterinary Research Centre (CECAV), University of Trás-os-Montes e Alto Douro, 5001-801 Vila Real, Portugal
[d] Associate Laboratory for Animal and Veterinary Sciences (AL4AnimalS), Portugal
[e] Department of Veterinary Sciences, University of Trás-os-Montes e Alto Douro, 5001-801 Vila Real, Portugal
[f] Biosckin, Molecular and Cell Therapies S.A., Laboratório Criovida, TecMaia, Rua Engenheiro Frederico Ulrich 2650, 4470-605 Moreira da Maia, Portugal
[g] Veterinary Clinics Department, Abel Salazar Biomedical Sciences Institute (ICBAS), University of Porto (UP), Rua de Jorge Viterbo Ferreira, n 228, 4050-313 Porto, Portugal
[h] Animal Science Studies Centre (CECA), Agroenvironment, Technologies and Sciences Institute (ICETA), University of Porto (UP), Rua D. Manuel II, Apartado 55142, 4051-401 Porto, Portugal
[i] University School Vasco da Gama (EUVG), Avenida José R. Sousa Fernandes, 3020-210 Lordemão, Coimbra, Portugal
[j] Vasco da Gama Research Center (CIVG), University School Vasco da Gama (EUVG), Avenida José R. Sousa Fernandes, 3020-210 Lordemão, Coimbra, Portugal
[k] Universidade Católica Portuguesa, Centro de Biotecnologia e Química Fina (CBQF), Laboratório Associado, Escola Superior de Biotecnologia, Rua de Diogo Botelho 1327, 4169-005 Porto, Portugal
[l] REQUIMTE/LAQV – Departamento de Engenharia Metalúrgica e Materiais, Faculdade de Engenharia, Universidade do Porto, Rua Dr Roberto Frias, 4200-495, Porto, Portugal

ARTICLE INFO

Keywords:
Dextrin
Injectable
Hydrogel
Bone regeneration
Stem cells
Dental pulp

ABSTRACT

Regeneration of severe bone defects remains a challenge. A formulation of synthetic glass-reinforced hydroxyapatite bone substitute, Bonelike® Poro (BL®P), 250–500 μm-diameter, with a dextrin-based hydrogel (HG), further loaded with human dental pulp stem cells (hDPSCs) with osteogenic differentiation ability, was tested for the management of critical-sized defects in an ovine model.

Morphology, calcium release, and mechanical strength of HG + BL®P were analyzed. Then, BL®P, HG + BL®P, and 10^6 hDPSCs-loaded HG + BL®P were implanted in ovine critical-sized 14 mm-diameter calvaria defects. Bone samples were collected after 3 and 6 weeks for histological and micro-CT analysis.

BL®P exhibits a suitable porous size for cell ingrowth, from the nm (>200 nm) to the μm (5 μm) range. The addition of BL®P granules to the HG resulted in increased compressive elastic modulus and ultimate tensile strength. The mildly acidic nature of the HG contributed to a faster dissolution of granules. In vivo results confirmed the HG suitability as a carrier, providing better defect filling, easy handling, and injectability of BL®P without compromising new bone formation nor biocompatibility. The HG + BL®P formulations can successfully regenerate critical-sized defects; however, addition of hDPSCs did not significantly enhance new bone formation under these conditions.

Granular BL®P provides an effective alternative to autologous grafts. The HG acts as a biocompatible carrier of granular bone substitutes and cells, conferring injectability and cohesivity.

Abbreviation: ADH, adipic acid dihydrazide; ANOVA, one-way analysis of variance; ARS, Alizarin Red S; BL®P, Bonelike® Poro; HA, Ca, calcium; DPBS, Dulbecco's phosphate-buffered saline; FBS, fetal bovine serum; FCT, Portuguese Foundation for Science and Technology; GAGs, Sulphated Glycosaminoglycans; GRAS, generally-recognized-as-safe; HA, Hydroxyapatite; HCL, hydrochloric acid; hDPSCs, human dental pulp stem cells; H&E, haematoxylin and eosin; HG, dextrin-based hydrogel; HLA-DR, human leucocyte antigen – DR isotype; ICP-OES, inductively coupled plasma optical emission spectroscopy; MSCs, multipotent mesenchymal stem cells; ODEX, oxidized-dextrin; ORO, Oil Red O; PBS, phosphate-buffered saline; PVA, polyvinyl alcohol; Circular Region of Interest, ROI; SD, standard deviation; RT-PCR, real-time polymerase chain reaction; SEM, Scanning Electron Microscope; TCP, Tricalcium phosphate; VOI, volume of interest.

* Corresponding author at: CEB - Centre of Biological Engineering, University of Minho, Campus de Gualtar, 4715-057 Braga, Portugal.
E-mail address: fmgama@deb.uminho.pt (M. Gama).

https://doi.org/10.1016/j.mtla.2023.101859
Received 20 January 2023; Accepted 26 July 2023
Available online 26 July 2023

1. Introduction

Bone substitutes can substantially improve life quality by repairing damaged bone, accelerating healing, avoiding complications, and improving outcomes, but they become absolutely indispensable in cases of critical-sized defects, defined as defects incapable of complete spontaneous regeneration during the entire lifetime [1]. A study report shows the global bone graft and substitutes market size was valued at USD 2.78 billion in 2020, being expected to grow at a rate of 5.8% from 2021 to 2028 [2]. Indeed, bone defect is a common event that may arise from numerous clinical circumstances related to, for instance, fractures, traumas, tumors, infections, and other disorders [3]. Incidence of these scenarios will likely be aggravated as a consequence of the increasing human life span. World Health Organization foresees the proportion of the world's population over 60 years to double from 12% to 22% between 2015 and 2050 [4].

In the management of bone defects, grafts have long been used to support bone deposition at the early stages of osteointegration, providing mechanical support, and a tuned resorption rate as synchronized as possible with new host bone replacement, being osteoconductive, osteoinductive and osteogenic so that new bone can grow within the biomaterial [3]. Hydroxyapatite (HA) is a bioactive ceramic, one of the most effective calcium phosphates used for the development of synthetic grafts for bone repair. This mineral mimics the composition of natural bone, is porous, osteoconductive, resorbable, biocompatible and shows good osseointegration, providing excellent conditions for tissue ingrowth [5]. We have been applying a glass-reinforced HA bone substitute of different granulometries, Bonelike®, for regenerative purposes [6–13]. Bonelike® Poro (B®LP) is a biomaterial with micro and macroporous interconnected architecture [14]. Contrasting with micropores which are an important factor for cell adhesion, macroporosity is defined as possessing pores with one of its dimensions larger than 10 μm [15] which, together with interconnectivity, favors vessel infiltration for blood supply, cell colonization, communication, migration and proliferation, exchange of water and nutrients [16]. Consequently, macroporosity also favors cell-mediated biomaterial resorption which, ideally, should not occur faster than new bone ingrow. Additionally, osteoblasts (sized 10 - 50 μm) show preference for >100 μm pores [16,17]. BL®P production method generates granules of sizes between 150 μm and 6 mm (approximately), being convenient for various clinical applications, from smaller to larger defects in dentistry and orthopedics. Recently, BL®P from 2000 to 5600 μm in diameter, with pore sizes ranging from 200 to 600 μm, enabled the regeneration of 17 mm diameter critical-sized lesions over 5 months of recovery, in an ovine model of iliac crest [14], performing comparably to the autograph technique parallelly tested. Synthetic grafts emerge to overcome limited sources, morbidity, and rejections associated with autographs or allographs.

Bone substitutes should provide mechanical stability and promote the healing process, ultimately being replaced by functional tissue through remodeling. However, the management of large defects, unsatisfactory vascularization, and shortcomings in reabsorption rates and biomechanical performances remain a challenge. The rate of resorption is of primordial importance as it dictates the duration of osteoconductive support essential for bone regeneration. Low resorption rates, such as those found in pure HA or bovine-sed bone substitutes (Bio-Oss®, Geistlich Biomaterials, Switzerland), can result in a number of complications, such as displacement of the graft materials, implant failure, foreign body reactions, chronic inflammation, soft tissue fenestrations and associated cysts, and lack of biodegradation requiring the removal of the bone graft material [18]. In this regard, new bone substitute materials associated with sodium alginate as a glue to fix the bone particles, Mega-TCP and Mega-oss, performed comparably to Bio-Oss® in terms osteoblast differentiation ability, though displaying higher resorption rates than those of Bio-Oss (24.4%, 15.3%, and 3.3%, respectively) [19]. On the other hand, synthetic TCP bone substitutes (e.g. Cerasorb®), with high resorption rates provide short-term mechanical stability, having been associated with longer healing times [20]. Given that de novo bone formation is dependent on a time-dependent synchronized vascularization and bone formation, resorption rate of bone substitutes becomes essential in bone tissue engineering strategies.

Grafts can be associated with other bioactive agents to modulate or boost the regenerative process. Human dental pulp stem cells (hDPSCs), present inside the dental pulp, are a type of self-renewing, multipotent mesenchymal stem cells (MSCs) with easy accessibility and suitable for cryopreservation, being attractive for clinical application. hDPSCs have low immunogenicity, and lack expression of human leucocyte antigen (HLA-DR) surface molecules [21], diminishing the risk of transplant rejection between species [22]. hDPSCs are auspicious for bone repair owing to their osteodifferentiation potential and secretion of important pro-regenerative biomolecules. They can generate osteoblasts [23], produce extracellular and mineralized matrix [24], and have shown higher proliferative capacity and alkaline phosphatase activity compared to the popularly used bone marrow-derived MSCs [25]. Although several critical-sized pre-clinical models have been used to demonstrate the regenerative potential of hDPSCs associated with synthetic scaffolds, they have been mainly performed in rats, whereas other close-to-human models, such as goats, sheep, or swine are still rare [26]. Sheep is a suitable pre-clinical model of novel osteogenic technologies for reasons such as ease of housing, compliance, docility, availability, life-span for long-term treatment processes, and sufficiently large bones to allow testing multiple conditions simultaneously. Bodyweight, the macrostructure and the turnover and bone modeling rate are similar to those of humans [27,28].

Currently, there are many clinical cases requiring bone filling materials but most commercially available grafts display limited handling properties. The combination of hydrogels with bone substitutes is a well-established trend that can not only confer injectability, moldability, non-invasive techniques and avoid early evasion of particles, but also act as a platform for cell colonization and as a carrier of bioactive molecules and cells, which can considerably improve the healing process. Dextrin ($(C_6H_{10}O_5)n$) is a glucose polymer predominately composed of α-(1 → 4) glycosidic bonds, derived from starch by partial hydrolysis - a natural, broadly available, renewable source. Dextrin is a smart option for therapy design for several reasons, for instance: i) nontoxic, accepted as a generally-recognized-as-safe (GRAS) food ingredient [29–33], and available in medical grade; ii) low molecular weight (<2800 g/mol) [34] below the renal filtration limit range (~30–50 kDa) [35,36], avoiding tissue accumulation; iii) biodegradable, as it can be enzymatically decomposed into glucose monosaccharides by blood α-amylases; iv) holds multiple reactive primary and secondary hydroxyl groups, suitable for conjugations or grafting strategies and other chemical reactions; and vi) low viscosity, which can be adjustable, to improve quality of shape-filling materials [37]. In this work, aldehyde-bearing dextrin spontaneously cross-linked with adipic acid dihydrazide (ADH) amine groups by Schiff base reaction, without any chemical initiator, was used [38]. An injectable in situ hydrogel (HG) is so obtained, capable of complete filling and molding to irregular defects. This network is gradually dismantled owing to the reversible nature of hydrazone bonds in water [39]. We have previously reported HG's suitability as a carrier of nanogels, cells, biomolecules, and granular ceramics [34,38,40–42] and also demonstrated the in vitro cyto- and genocompatibility [38,43].

In a previous study, microporous BL®P (250–500 μm) associated with hDPSCs improved bone regeneration in a non-critical ovine model [44]. In this work, the same macroporous BL®P associated with HG will be used as a transplantation-based strategy for hDPSCs and tested in ovine critical-sized calvaria defects. Bone formation and biomaterial resorption will be analyzed at weeks 3 and 6 post-treatment through histologic and micro-CT processing. The aim of this study is to propose the HG as a delivery agent for hDPSCs, and also as an injectability-conferring agent, without compromising the regeneration

process provided by BL®P.

2. Material and methods

2.1. Materials and reagents

Dextrin used in this study was Tackidex B 167 (Batch E 1445), was kindly provided by Roquette (Lestrem, France). Sodium *m*-periodate, diethylene glycol, adipic acid dihydrazide (ADH), silver nitrate, sodium thiosulfate, dexamethasone, ascorbic acid-2-phosphate, β-glycerophosphate, Alcian Blue, acetic acid, sodium carbonate (Na_2CO_3), calcium fluoride (CaF_2), calcium hydrogen phosphate ($CaHPO_4$), diphosphorus pentoxide (P_2O_5) and polyvinyl alcohol (PVA), formaldehyde, pepsin and hydrochloric acid (HCl) were purchased from Sigma-Aldrich (St. Louis, MO, USA). Dulbecco's phosphate-buffered saline (DPBS), αMEM, fetal bovine serum (FBS), streptomycin, penicillin, and amphotericin B were obtained from Gibco® (Waltham, MA, USA). BL®P granules (250–500 μm) were provided by Biosckin—Molecular and Cell Therapies, S.A. Trypan Blue™ exclusion assay was purchased from Invitrogen™, for use with the Countess™ Automated Cell Counter Invitrogen™.

2.2. Preparation of dextrin-based hydrogel

First, dextrin was oxidized as previously described by our group [41]. Briefly, sodium *m*-periodate ($NaIO_4$), was added to dextrin solution (2% w/v), at an equivalent theoretical degree of oxidation of 40% (mol). The reaction was left stirring for 20 h at room temperature, protected from light, until stopped with a $NaIO_4$-equimolar amount of diethylene glycol. $NaIO_4$ and diethylene glycol were removed by dialysis (1000 Da cut-off membrane from Merck Millipore, USA) over 48 h with, and the dialyzed product, oxidized-dextrin (ODEX) was freeze-dried. Then, dextrin-based hydrogel was prepared as described by Pereira et al. [43]. ODEX solution was prepared in phosphate-buffered saline (PBS) buffer (30% w/v) and sterilized by gamma irradiation (20 kGy; 2 kGy/h), by IONISOS (Dagneux, France). ADH solution was prepared in PBS buffer as well (3.76% w/v) and sterilized by filtration with a 0.22 μm pore filter membrane (Pall Corporation, USA). ODEX and ADH solutions were used in a volume ratio of 7:3 to prepare *in vivo* formulations.

2.3. Preparation of Bonelike® Poro

BL®P was prepared as previously reported [45,46]. Briefly, HA powder and P_2O_5-CaO-based glass were individually prepared and mixed. To prepare P_2O_5-CaO phase, appropriate quantities of Na_2CO_3, $CaHPO_4$, CaF_2, and P_2O_5 were mixed and heated up to 1450 °C, for 90 min, in a glass furnace and poured into deionized water, then crushed in an agate mortar and sieved to obtain a fine glass powder with a particle size below 50 μm. BL®P was obtained by mixing 2.5 wt.% of this glass powder with 97.5 wt.% of HA, and then further mixed with pore-forming agents, microcrystalline cellulose and polyvinyl alcohol, to obtain the micro and macroporous structure. The resulting mixture was dried at 60 °C for two days and samples were sintered at 1300 °C for 1 h, using a heating rate of 4 °C/min, then milled to the desired granule size. BL®P of 250–500 μm granule size was obtained, displaying a macroporous structure with interconnective porosity. Table 1 shows BL®P composition and properties were characterized by chemical analysis, X-ray diffraction (phases quantification), scanning electron microscopy (morphology), and mercury porosimetry (porosity).

2.4. Bonelike® Poro dissolution behavior

The dissolution behavior of BL®P was determined by measuring the concentration of calcium (Ca) ions released into solution, using inductively coupled plasma optical emission spectroscopy, ICP-OES (Optima 8000, PerkinElmer). In short, the dissolution rate was measured by immersing BL®P (30 ± 0.2 mg) in PBS buffer (without Ca^{2+} and Mg^{2+}, BioConcept Ltd.) pH 7.2, and in ODEX solution (30% p/v) with PBS in a 7:3 ratio at pH 5.2, i.e., using the HG components without ADH, to prevent gelling, at 37 °C, under mild agitation. Samples ($n = 5$) were collected at defined time-points, then diluted with ultra-pure water, filtered through a membrane with a 0.22 μm pore size and a few drops of nitric acid, HNO_3, (Fisher, Loughborough, UK, 69%) were added before analysis. A standard curve between 0.05 mg/L and 40 mg/L was prepared in nitric acid (5%) and plotted before analyzing samples. The operating conditions of ICP-OES were as follows: RF (radio frequency) power: 1400 W, argon plasma flow: 12 L/min, auxiliary gas flow: 0.2 L/min, nebulizer gas flow: 0.7 L/min. The plasma view was axial and the wavelength used for Ca analysis was 317.933 nm.

2.5. Mechanical test

Mechanical properties of empty or BL®P loaded HG samples were analyzed by uniaxial compression measurements on a TA HD Plus Texture Analyzer (Stable Micro Systems, UK), using a 25 mm aluminum probe. Test samples (5 mm thickness × 12 mm diameter) were poured into cylindrical molds and left crosslinking for 30 min before analysis. The force used to compress 70% of the initial height was measured at a speed rate of 0.5 mm/s. A trigger force of 1 g was used. The rupture point was evaluated by the maximum peak of the stress–strain curve, and Young's modulus (E) was determined as the average of the slopes of the first linear interval in the range between 2 and 7% deformation of the stress–strain curve. Tests were performed in triplicate.

2.6. Scanning electron microscopy

Dried BL®P granules before and after 15 days of immersion in PBS or ODEX were added to aluminum pin stubs with electrically conductive carbon adhesive tape (PELCO Tabs™) and 25 angstroms Au coated. The coated samples were then placed on a Phenom Standard Sample Holder and characterized using a desktop Scanning Electron Microscope (SEM) (Phenom ProX, Netherlands) at 15Kv. All resulting images were acquired using the ProSuite software v.3.0.

2.7. Human dental pulp stem cells (hDPSCs) culture and characterization

Cells were obtained from AllCell, LLC (Cat. DP0037F, Lot No. DPSC090411-01) and cultured under standard conditions (37 °C, 95% humidified atmosphere and 5% CO_2) with αMem (32,561,029, Gibco®), supplemented with 10% FBS (A31608–02, Gibco®) and 100 IU/ml penicillin, 0.1 mg/ml streptomycin (15,140,122, Gibco®), 2.05 mg/ml amphotericin B (15,290,026, Gibco®). We have previously shown hDPSCs differentiation ability towards the osteogenic, chondrogenic and adipogenic cell lineages, and further MSCs' phenotype identification, assessed by flow cytometry and real-time polymerase chain reaction (RT-PCR) [41,47].

Table 1
Composition and properties of BL®P.

Material	Ca/P ratio	HA (%)	α-TCP (%)	β-TCP (%)	Ions	Granules size (μm)	Surface area (m^2/g)	Porosity (%)
BL®P	1.70	75 ± 2	15 ± 2	8.0 ± 1.1	Ca^{2+}, PO_4^{3}, F^{-}	250–500	7.237	65

HA, Hydroxyapatite; BL®P, Bonelike® Poro; TCP, Tricalcium phosphate.

Each cell dosage was composed of 10^6 viable hDPSCs at passage 4, suspended in 0.05 mL DPBS (14,190,144, Gibco®). Cell viability was assessed using the Trypan Blue™ exclusion assay, after trypsinization of the cells at passage 3. Cell population presented approximately 98% viability after trypsinization. Cell dosages of 10^6 viable hDPSCs were prepared in DPBS, immediately prior to in vivo application.

2.8. Preparation of formulations for in vivo implantation

To reach a final HG volume of 500 μL, 150 μL of ADH (3.76%, w/v) and 350 μL of ODEX (30%, w/v) were aliquoted separately. BL®P granules (0.29 g) were distributed in microtubes, representing 60% (w/v) of the hydrogel (w_{BL}/v_{HG}). A dose of 10^6 of hDPSCs were used per formulation. Cells were thawed and washed by centrifugation (270 g, 7 min) with culture medium to eliminate the cryoprotectant, dimethyl sulfoxide, and then washed with PBS to eliminate fetal bovine serum present in the culture medium, to avoid any undesired reaction. The final pellet was resuspended in 50 μL PBS. Formulations were prepared according to Table 2. When used without HG, BL®P granules were mixed with autologous blood prior to application. For injectable samples, BL®P granules were poured into ODEX solution and 50 μL of cell suspension in PBS were then added. ADH was mixed for crosslinking reaction, which took 20 to 30 min until a properly gelled and mouldable paste was achieved. For HG + BL®P formulation, 50 μL of empty PBS was added in substitution of cell suspension. The preparation and handling details are represented in Fig. 1.

2.9. Surgical procedure

All procedures were in conformity with the Directive 2010/63/EU of the European Parliament and Portuguese legislation (Portaria 1005/92), and with the approval of the Portuguese Veterinary Authorities (Direção-Geral de Alimentação e Veterinária). Ovis aries (churra da terra quente sheep) were included this study: 10 healthy nonpregnant adult female individuals, with an average weight of ~40 kg and aged between 7 and 8 years. Animals were randomly sacrificed at weeks 3 and 6, 5 animals per time-point for bone deposition analysis. In each animal, four identical defects were performed in the calvaria and randomly filled with different formulations, as follows: i) no treatment (control); ii) BL®P; iii) HG + BL®P and iv) HG + BL®P + hDPSCs (Fig. 1). Block randomization was used to allocate the different conditions. The animals were pre-medicated with 0.1 mg/kg acepromazine (Calmivet®, Vetoquinol) and 0.01 mg/kg buprenorphine (Bupaq®, Richter Pharma AG), with anesthesia induction performed with 0.25 mg/kg diazepam (Labesfal), 5 mg/kg ketamine (Ketabel®, Bela-pharm) and 4 mg/kg propofol (lipuro®, Bbraun). Endotracheal intubation was performed by direct visualization using a rigid endoscope placed inside the endotracheal tube. Surgeries were conducted under inhaled general anesthesia using isofluorane and intravenous fluid was provided at maintenance rate (NaCl 0,9% B Braun®). The skin was prepared by performing wool shaving and antisepsis with chlorhexidine 4% and an incision was made along the sagittal plan from the base of the horns until the middle of the nasal bone, so that defects could be made in the calvaria. The periosteum was opened and full thickness critical-sized bone defects were performed in the frontal bone with a trephine (outer ∅ 14 mm) overlying the frontal sinus, leaving the sinus mucosa and its fibrous connections intact. During this procedure, the bone was continuously irrigated with saline solution in order to avoid overheating and consequent bone necrosis. HG formulations were then placed in the defect with a syringe, excepting for the HG-depleted BL®P sample that was mixed with autologous blood. All treatments were sculpted within the defect with a spatula. Periosteum and soft tissues were closed in layers with resorbable sutures in a continuous pattern and the skin with an intradermic suture. The animals were set free and received analgesic medication for 4 days, with flunixin meglumine and antibiotic treatment for 7 days with amoxicilin. Animals were sacrificed with a lethal intravenous injection of 40% sodium pentobarbital (Euthasol®). The frontal bones were removed from the head using an oscillating saw, a hammer and an osteotome and then fixed in 4% formaldehyde solution and X-ray images were obtained. Then, each bone defect was sectioned using an oscillating saw and maintained in formaldehyde until analysis.

Table 2
Composition of formulations applied in vivo.

Formulation	BL®P (60% WBL/VHG)	hDPSCs	ODEX (30% w/v)	ADH (3.76 w/v)
BL®P	0.29 g	–	Autologous blood	
HG + BL®P	0.29 g	50 μL PBS	350 μL	150 μL
HG + BL®P + hDPSCs	0.29 g	10^6 cells in 50 μL PBS	350 μL	150 μL

BL®P, Bonelike Poro; HG, hydrogel; hDPSCs, human dental pulp stem cells; ODEX, oxidized-dextrin; ADH, adipic acid dihydrazide.

2.10. Micro-computed tomography analysis

The micro-CT images of the collected samples were obtained using SkyScan 1275 equipment (source voltage 80 kV and source current 125 uA and with an acquisition time of 45 min) (Bruker, Karlsruhe, Germany). The images were reconstructed using Nrecon 1.7.5.0 software. For data analysis, samples were first aligned perpendicular to the skull surface and a volume of interest (VOI) with 300 slices was defined using DataViewer 1.5.6.3 software. Then, using CTanalyser 1.18.10.0 software, a Circular Region of Interest (ROI) with a diameter of 13.9 mm was determined (Fig. 2). The cut to start the data analysis was determined by the first lower cut that presented a closed bone circle. In order to characterize the different types of components existing in the samples three thresholds were defined: the one characterizing the ceramic granules (170 / 255); the one characterizing the previously existing bone (110 / 160) and the one characterizing the newly formed bone (85 / 255). The data analysis was performed firstly by subtracting in the ROI the existing bone with the 110 / 160 threshold and then determining the presence of granules with the 170 / 255 threshold and the formation of new bone with the 85 / 255 threshold.

2.11. Histological analysis

Bone samples kept in formaldehyde solution were decalcified with Surgipath decalcifier II (Leica Biosystems, USA), for at least 5 days, dehydrated and embedded in paraffin wax, in an automatic tissue processor Hypercenter XP (Shandon®, GMI Trusted Laboratory Solutions, USA). Consecutive 3 μm sections were cut and stained with haematoxylin and eosin (H&E) and Masson's trichrome. Images were acquired using a Nikon VR microscope connected to a Nikon VR digital camera DXM1200.

2.12. Statistical analysis

Experimental data were presented as mean ± standard deviation (SD). Statistical analysis of data was performed by one-way analysis of variance (ANOVA) followed by the Tukey's post-test, a value of $p < 0.05$ (*) was considered to be significant, except for the mechanical test in which a student's *t*-tests was used. Shapiro–Wilk test was applied as a normality test. The analysis was performed using Prism Graph Pad 8.0.2 software® (Graph Pad Software, La Jolla, CA, USA).

3. Results

3.1. Human dental pulp stem cells characterization

hDPSCs used in this experiment were previously characterized and published [44]. Figure 3 shows hDPSCs morphology cultured at passage

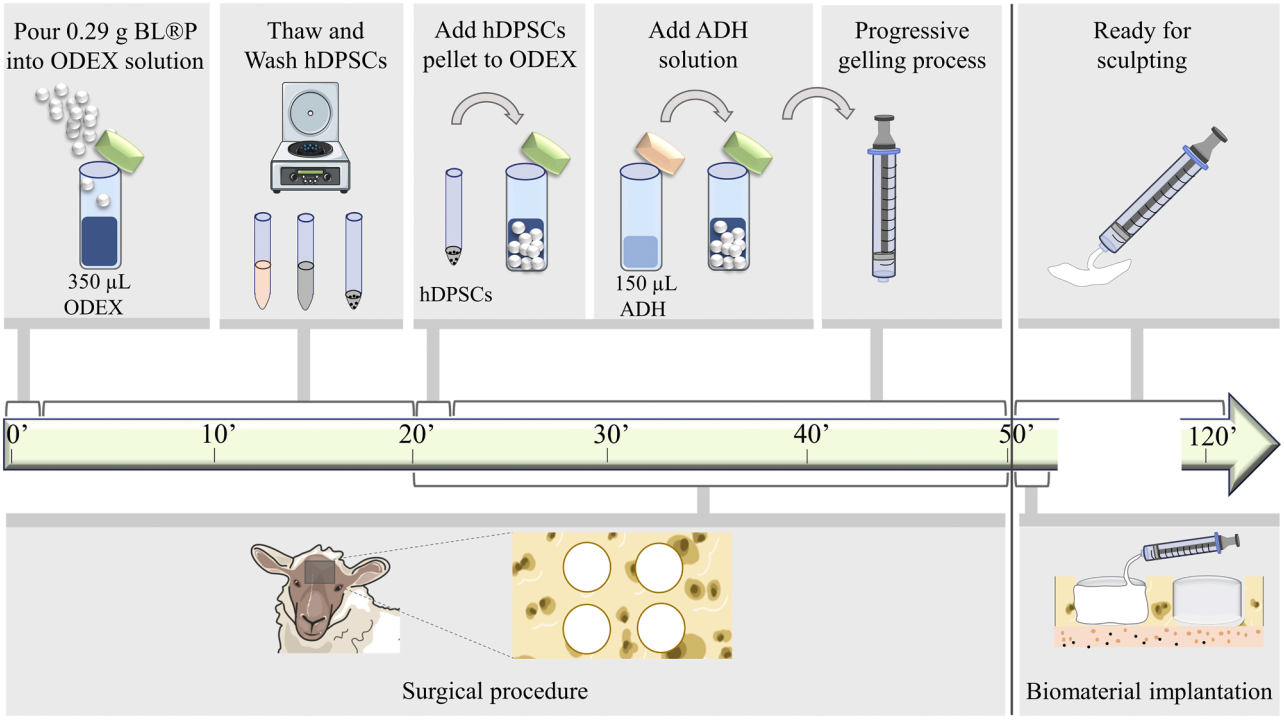

Fig. 1. Sequence of events demonstrating preparation and handling of hydrogel formulations, accompanying the surgical procedure time length. ODEX, oxidized-dextrin; ADH, adipic dihydrazide; hDPSCs, human dental pulp stem cells. (2-column fitting image; color).

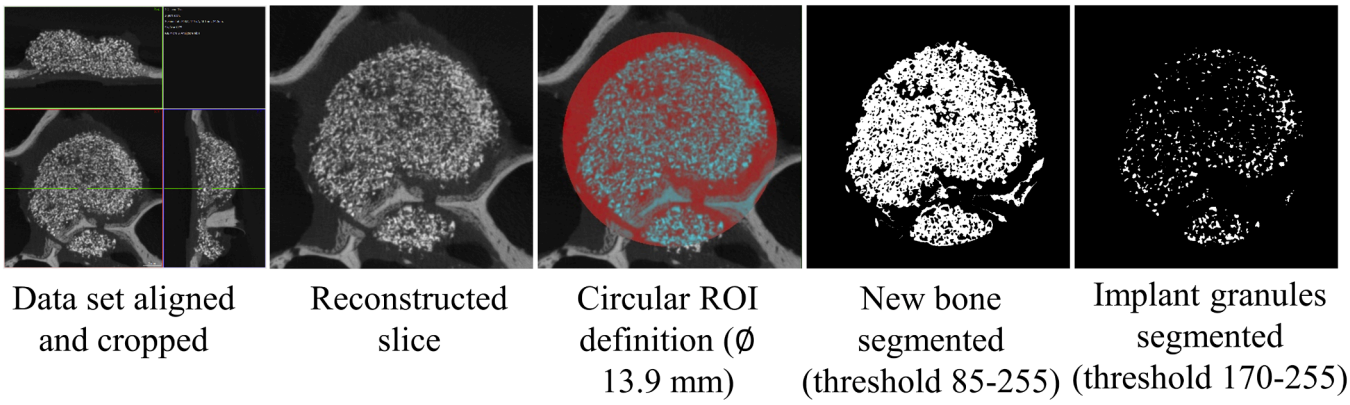

Fig. 2. Micro-CT protocol visually exemplified. (2-column fitting image; color).

3. Briefly, hDPSCs were demonstrated to present characteristic hMSCs' markers, as assessed through flow cytometry. Over 90% of the population was positive for CD90, CD105 and CD44, and ≤2% were negative for CD34, CD11b, CD19, CD45 and MHC II. Gene expression was performed through RT-qPCR analysis. Total RNA was successfully extracted from cultured hDPSCs and specific gene expression was assessed. CD34 was not detected, as expected for hDPSCs. CD105, CD73 and CD90 were highly expressed; CD166, MHC I and CD117 showed strong to moderate expression. Multipotency genes as Nanog, Oct4, Sox2, were also weakly expressed (Delta threshold cycle value >35). Moreover, weak expression of MHC class II was detected in hDPSCs by RT-qPCR analysis, however, membrane expression demonstrated by flow cytometry, was not detected. Tri-lineage differentiation was quantitatively evaluated through Oil Red O (ORO), Alizarin Red S (ARS) and Sulphated Glycosaminoglycans (GAGs) protocols, to evaluate adipogenic, osteogenic and chondrogenic differentiation, respectively. Results demonstrated successful differentiation towards the three lineages, with significant differences from undifferentiated controls. Particularly relevant was the capacity for osteogenic differentiation, proven both qualitatively through alizarin red staining and quantitatively through alizarin red staining quantification, a concentration that showed statistically significant differences with the control group, that is, hDPSCs not subjected to osteogenic differentiation medium. The RT-PCR technique also allowed to identify the osteogenic activity marker ALP, with ΔCt values higher than those identified in other MSCs such as those derived from the umbilical cord.

3.2. *Dissolution rate, morphology and mechanical behavior*

Despite being mostly composed of HA, BL®P also possesses α-TCP and β-TCP phases (table 1) which are much more soluble than HA. The dissolution rates of BL®P at different pH are summarized in Fig. 4. In the weak acidic ODEX solution (pH 5.2), simulating the hydrogel pH environment, BLP released Ca^{2+} ions at a faster rate compared to PBS (pH 7.2). Figure 5 shows the BL®P morphology, exhibiting irregular structure with interconnected macropores from the nm (>200 nm) to the µm range at 4500× magnification. No significant morphological differences

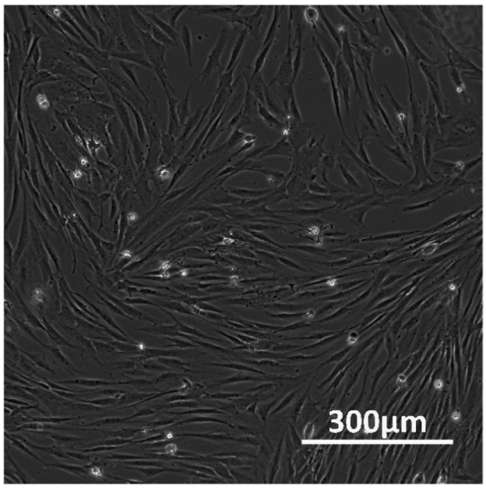

Fig. 3. Human dental pulp stem cells (hDPSCs) cultured at passage 3, with a ~90% confluency, prior to trypsinization, cell viability assessment by the Trypan Blue™ exclusion assay, and dosage preparation. (Single column fitting image).

were seen after 15 days of dissolution.

A compressive test was performed on HG and HG + BL®P formulations with 5 mm thickness and 12 mm in diameter (Fig. 6). The addition of BL®P to the HG increased its Young's modulus and maximum compressive strength, from 0.163 ± 0.040 kPa to 0.400 ± 0.137 kPa and from 66.8 ± 6.5 kPa to 163.3 ± 13.2 kPa, respectively (Table 3). The HG + BL®P presents better mechanical properties, but insufficient to confer relevant load bearing ability to the composite.

3.3. Surgical analysis

The surgical procedure was simple and well tolerated by the animals. The HG formulations were convenient to handle and administered in one step, perfectly shaping to the defects up to the edges, without leaking granules. On the contrary, BL®P previously mixed with autologous blood, was implanted with a surgical spatula little by little, until complete defect filling, each time gently compressing in an attempt to stick the material together and prevent leakage out of the defect. Gelling time refers to the moment when samples become sticky enough as to properly being implanted without leakage. The more time, the stickier or harder the sample becomes. The addition of hDPSCs pellet (or empty PBS) to the pre-stablished 7:3 (v/v) (ODEX:ADH) HG formulation, diluting the sample, culminated in a gelling time around ~25 to 30 min, with no influence on handling, sculpting, cohesivity, injectability or any other formulation feature. A representative final aspect of the implantation sites is shown on Fig. 7A and that of the harvested bone after the fixation process on Fig. 7B. The post-surgery period was free of any complications (infections, abscesses or allergic reactions), and the surgical skin incision healed as expected. Also, no evidence of adverse tissue reaction nor infection were detected during bone sample harvesting.

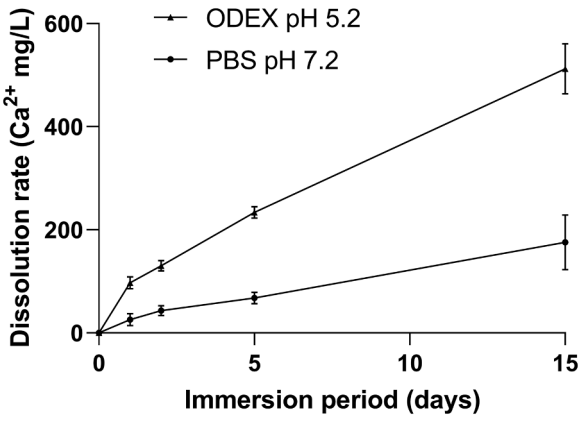

Fig. 4. Dissolution of Bonelike® Poro (BL®P), expressed as the amount of calcium ions release as a function of time in oxidized-dextrin (ODEX) solution pH 5.2, and phosphate-buffered saline (PBS) buffer pH 7.2, up to day 15. Data are presented as mean ± standard deviation (n = 5). (Single-column fitting image).

3.4. Bone regeneration of critical-sized defects

3.4.1. Micro-computed tomography analysis

Implantation sites were examined 3- and 6-weeks post-treatment. Micro-CT analysis provided visual proof of bone deposition in the whole implanted area in each time-point, further enabling the distinction between new bone and remaining granules (Fig. 8). Control condition was not able to regenerate over time, presenting scarce and small ossification focus, whereas all the three BL®P treatments displayed considerable bone deposition. These conditions achieved an almost complete osteointegration up to week 6, excepting for the peripheral area and, in the case of HG formulations, few interspersed empty areas.

The effect of the addition of the HG or hDPSCs to BL®P formulations can be more precisely distinguished in Fig. 9(A) and (B), where the volume of new bone, granules and total bone were quantified in mm^3 (n = 5). New bone and total bone volumes were not significantly different among treatments with and without HG, for both time-points, which demonstrates that the HG does not compromise the formation of new bone. These results also show that hDPSCs loaded into the HG and BL®P did not significantly enhance new bone formation for the specific conditions used and up to week 6 of tissue repair, though a tendency for more bone ingrowth may be denoted at early stage compared to the HG + BL®P formulation. At week 3, the remaining amount of granules was higher in the BL®P condition, as compared to the HG formulations (although not statistically significant - Fig. 9(C)), which suggests a faster resorption in the presence of the HG, as shown previously on Fig. 4. At week 6, the remaining granules are present in similar amounts for all formulations; although a trend towards lower amount of granules over time (week 6 versus week 3) is apparent, the difference is not significant, due to the low absorption rate of the biomaterial.

3.4.2. Histological analysis

The tissue obtained after regeneration was further analysed histologically. Figures 10 and 11 show H&E and Masson's trichome staining, respectively. Three weeks post-surgery, defects without treatment (control) show dense connective tissue with scattered inflammatory cells and no signs of bone formation. Usually, all treatments presented new trabecular bone interspersed with connective tissue circling the granules, evidencing the presence of osteoblasts, osteoclasts and vessels. BL®P group induced a faster regenerative process, evidencing notorious mature bone with well differentiated osteocytes. Both the addition of HG and hDPSCs to BL®P granules showed no benefit in terms of bone formation at week 3, according to micro-CT analysis (Fig. 9). Macrophage activity was detected around a material suspected being HG remains.

At week 6, non-treated group confirmed the difficulty on developing new bone as expected for a critical-sized defect, showing dense connective tissue with few minor focus of ossification. Groups with HG+BL®P and HG+BL®P+hDPSCs evidenced the presence of larger amounts of mineralized bone (magenta color on Masson's trichome stain) spread throughout almost the entire defect, engulfing granules of smaller size, accompanied by a decrease in fibrous tissue, as compared to week 3. The groups treated with BL®P granules presented several new vessels circling the biomaterial. No signs of HG remains was noticed at this stage. Overall, the addition of HG and cells did not compromise nor accelerate bone formation, respectively.

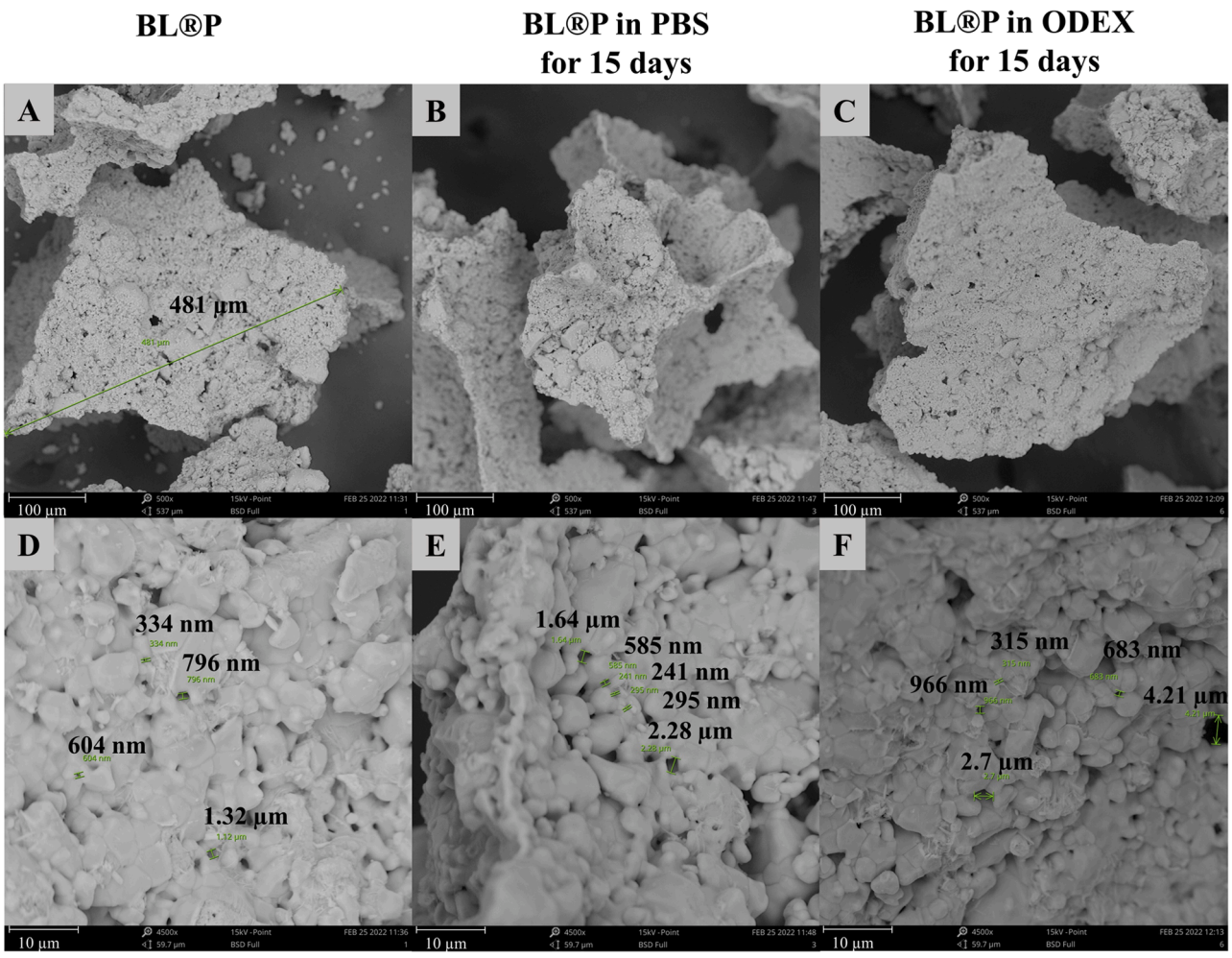

Fig. 5. SEM images of (A and D) Bonelike® Poro (BL®P) granules before immersion, (B and E) BL®P after 15 days of immersion in PBS solution and (C and F) in oxidized-dextrin (ODEX) solution. Macropores of BL®P are indicated by green arrows (A to C: 500× magnification, scale bars = 100 µm, E to G: 4500× magnification, scale bars = 10 µm). (2-column fitting image; color).

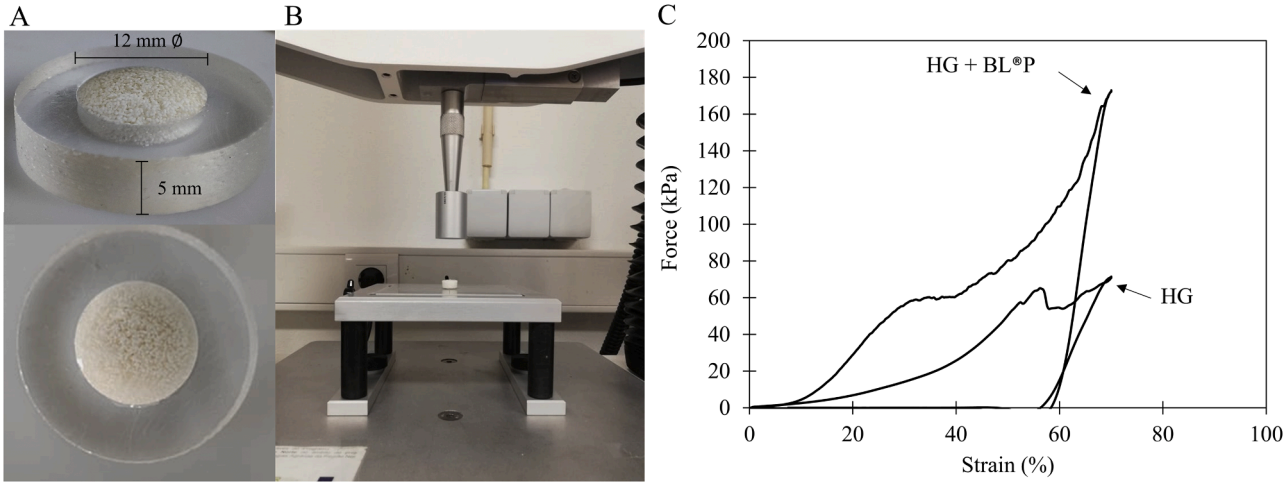

Fig. 6. Compressive test: preparation of (A) disc-form HG + BL®P material in 12-diameter molds before (B) positioned under the probe, and (C) stress–strain curves for HG and HG + BL®P formulations. Data are presented as mean ± standard deviation ($n = 3$). (2-column fitting image; color).

4. Discussion

We hereby show the regeneration of full-thickness 14 mm Ø critical-sized defects performed in the calvaria of an ovine model, using a synthetic glass-reinforced HA bioceramic associated to an HG, further loaded with hDPSCs. Main features of the formulation include ease of preparation and administration, safety validation and bone deposition after 3 and 6 weeks of treatment.

Table 3
Compressive modulus, stress (at 70% strain) for HG and HG + BL®P formulations. Data are presented as mean ± standard deviation (n = 3). Statistical analysis was performed using unpaired student's t-test.

Sample	Young's modulus (E) [kPa]	Maximum compressive strength [kPa]
HG	0.163 ± 0.040	66.8 ± 6.5
HG + BL®P	0.400 ± 0.137	163.3 ± 13.2
p value	0.0452	0.0003

Calcium ions release was nearly 3 times higher in acidic ODEX solution than in PBS at day 15, therefore expected to result in a faster BL®P dissolution rate in vivo. We have previously observed this outcome in other dextrin-based HG reinforced Bonelike® formulations applied in vivo [41]. How this release of calcium ions may affect the viability and proliferation of hDPSCs was not specifically explored in this work, and it would be important to analyze this factor in vitro in the future, although the fact that the presence of hDPSCs did not accelerate formation bone until week 6 with the presence of ODEX seems to indirectly indicate that there is no effective influence on cellular performance. The dissolution behavior of HA and TCP-based bone substitutes in weak acidic solution, mimicking Howship's lacunae, has been shown to be faster compared to

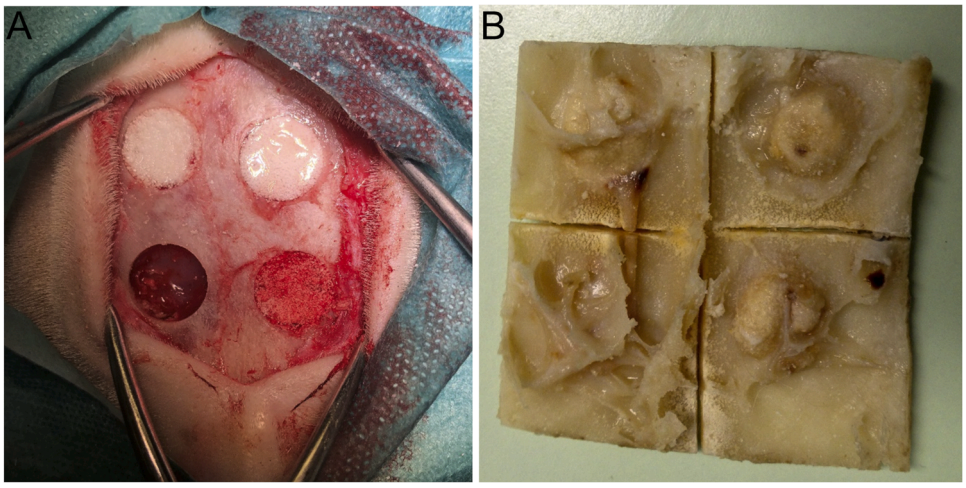

Fig. 7. (A) Frontal bone critical-sized defects performed in sheep, fulfilled with formulations: control (left-bottom); Bonelike® Poro (BL®P) mixed with autologous blood (right-bottom); dextrin-based hydrogel (HG) + BL®P + human dental pulp stem cells (hDPSCs) (left-upper) and HG + BL®P (right-upper). (B) Harvested frontal bone after fixation. (1.5-column fitting image; color).

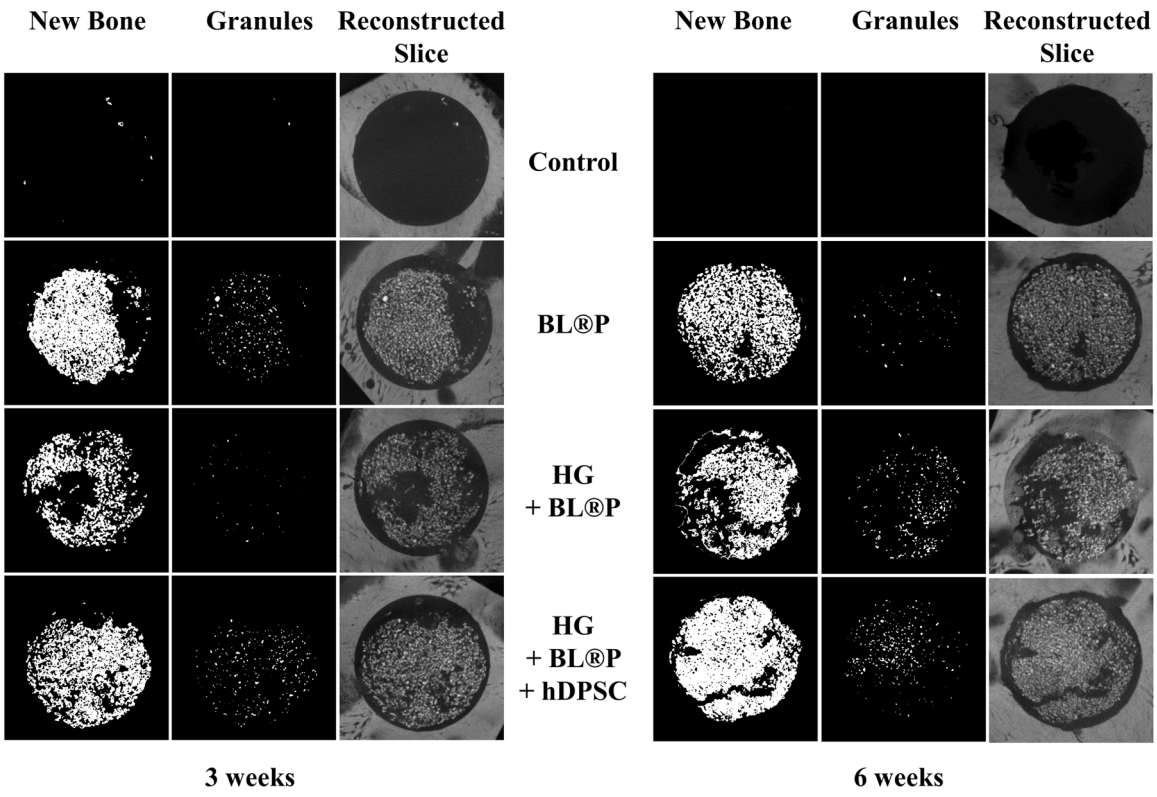

Fig. 8. Representative micro-CT slice images of the implantation sites after 3 and 6 weeks of treatment with different formulations. (2-column fitting image).

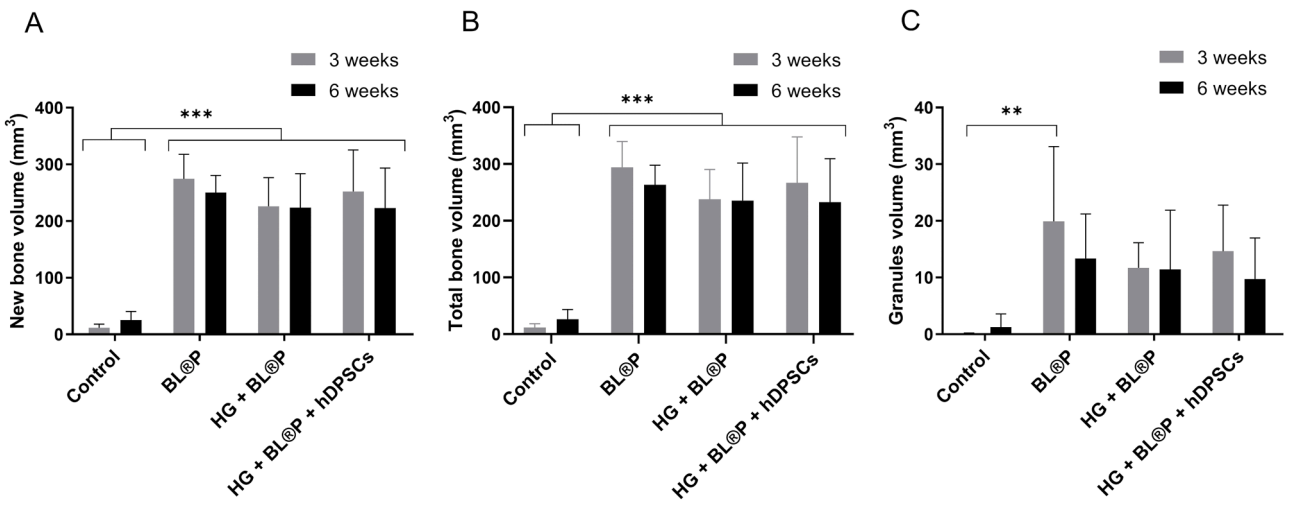

Fig. 9. Quantification of the new bone (A), total bone (B) and granules (C) volumes in implanted sites after 3 and 6 weeks of treatment. Total bone refers to the sum of new bone with granules. Statistical analysis was performed within each time-point using one-way analysis of variance (ANOVA) followed by the post-hoc Tukey test (** $p < 0.01$ and *** $p < 0.001$). Results are shown as mean values ± standard deviation ($n = 5$). BL®P, Bonelike® Poro; HG, hydrogel; hDPSCs, human mesenchymal stem cells. (2-column fitting image).

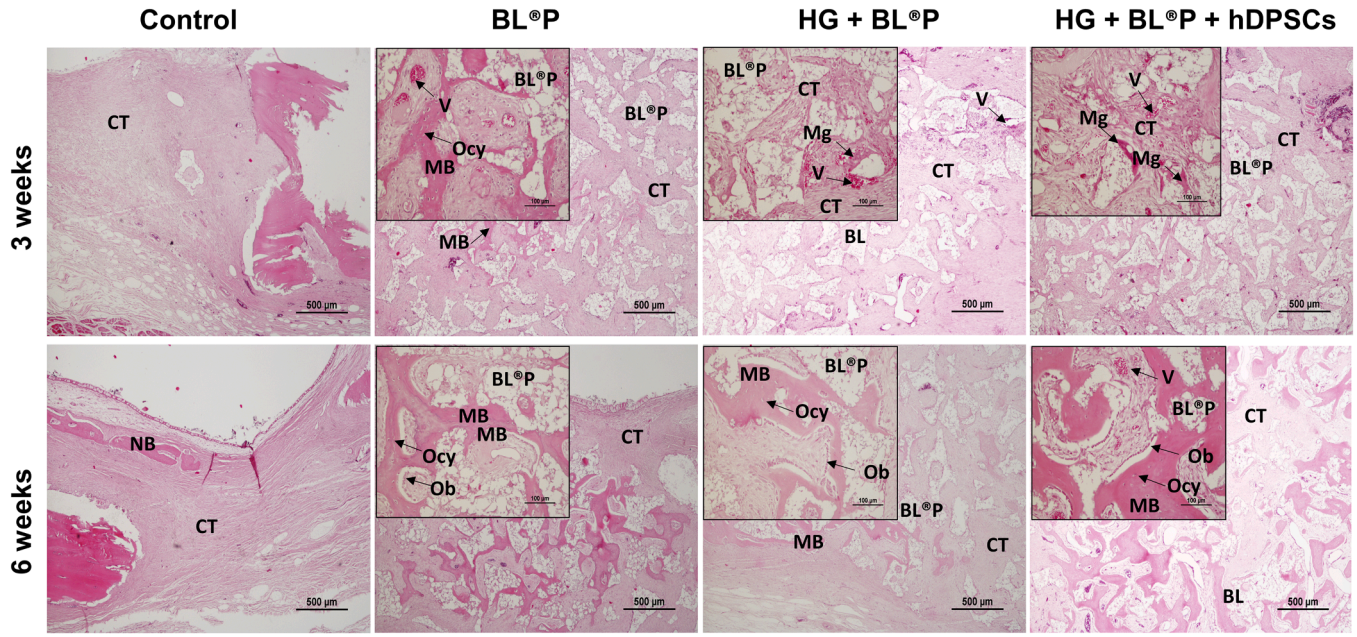

Fig. 10. Haematoxylin- and eosin-stained histological sections from implanted sites after 3 and 6 weeks of treatment. CT, connective tissue; BL®P, Bonelike®Poro granules; NB, new bone; V, vessel; Ob, osteoblasts; Ocy, osteocytes; MB, mature bone; Mg, macrophage. Scale bar 500 µm (larger images) and 100 µm (smaller images). (2-column fitting image; color).

physiological solution, mostly owing to the TCP phase [48]. Though, significant morphological differences could not be noticed microscopically for up to 15 days of immersion. The HG exhibits a soft structure, and the incorporation of ceramic granules increased the stiffness of the material, providing a more stable 3D shape where granules are homogeneously distributed within the bone defect. Stability of the 3D shape can be important to avoid defect collapse. Young's modulus and maximum compression strength increased by nearly 2.5 times by adding the mineral phase to the HG, though the material is still soft and moldable enough to fit non-regular shapes. Indeed, the addition of ceramic particles to hydrogels has been reported to reinforce mechanical properties simultaneously exhibiting moldability [17]. Hydrogel stiffness has been shown to have major impact on MSCs differentiation and fate [49–51], playing a major role in fracture healing. The spreading capacity of umbilical cord MSCs and expression of osteoblastic makers were shown to be stronger as the stiffness of polyacrylamide gels increased (Young's modulus: 13–16, 35–38, 48–53, and 62–68 kPa) [50]. The interplay between biomaterial composition, stiffness and cellular response should therefore be customized. Since this matter is highly target-specific, comparisons with data from the literature is not straightforward. In our case, ODEX HG may be customized by adjusting the HG to BL®P ratio or degree of crosslinking.

The surgical process was free of any complications. The administration of BL®P was more convenient when associated to the HG, which molded granules (250–500 µm) into a cohesive paste-like material suitable for injectability, within 25 to 30 min. The HG formulations were applied in one step without granules leakage, while granules embedded in blood required a multiple step administration-and-sculpt process. The

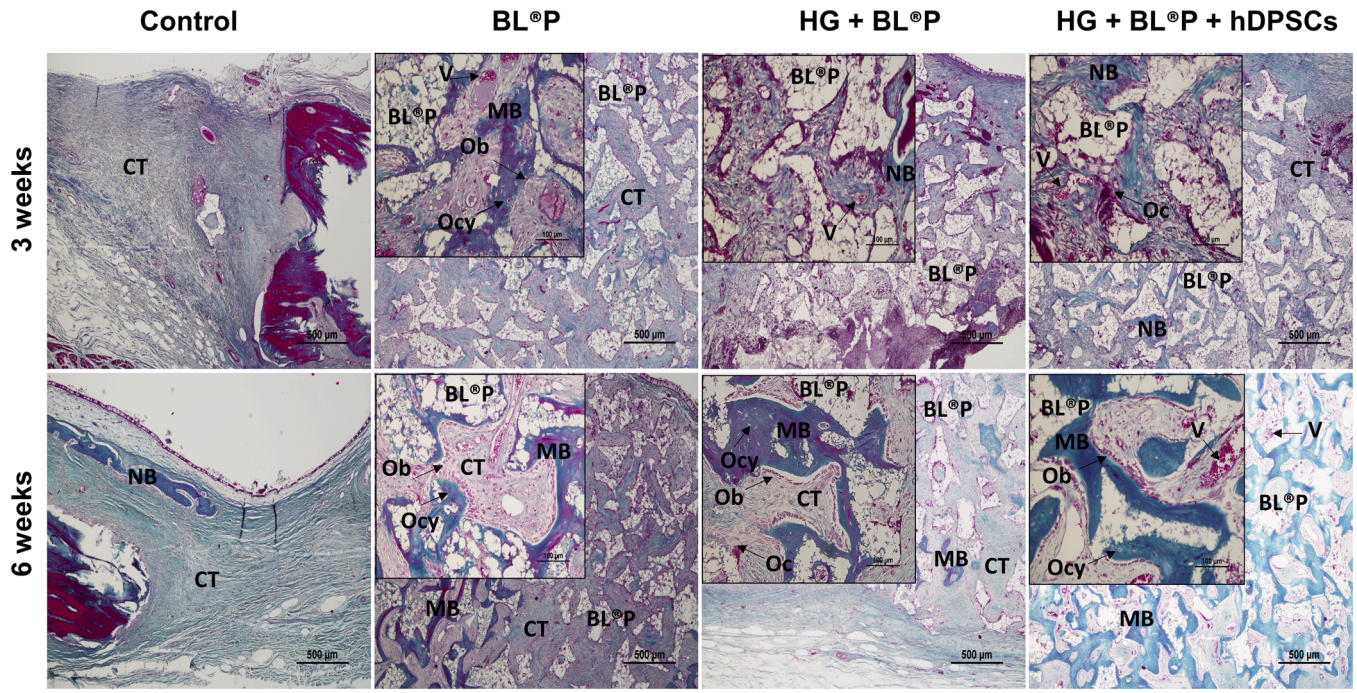

Fig. 11. Masson's trichrome-stained histological sections from implanted sites after 3 and 6 weeks of treatment. CT, connective tissue; BL®P, Bonelike®Poro granules; NB, new bone; V, vessel; Ob, osteoblasts; Oc, osteoclasts; Ocy, osteocytes; MB, mature bone. Scale bar 500 µm (larger images) and 100 µm (smaller images). (2-column fitting image; color).

addition of cells (or PBS) to the BL®P and HG components slightly delayed the gelling time by around ~10 min. The HG formulation is, therefore, suitable for holding small volumes of water-based bioactive agents, particularly those requiring immediate administration upon preparation, whereas autologous blood would not serve this purpose. In an attempt to deliver and retain Bonelike® granules and hDPSCs, fibrinogen and thrombin-based TISSEEL Lyo® glue of human origin was used in another work, evidencing the need for a vehicle or handling tool for this type of grafts [44]. Although generally safe, products derived from human blood cannot exclude the possibility of transmitting infections, or generate allergic or hypersensitivity reactions as with any protein-containing products. TISSEEL Lyo® mimics physiological clot and can only been applied topically or epilesionally as a thin layer, to maintain efficacy and avoid interference with the healing process, being also inadequate for injecting, as stated in the product's data sheet.

A 14 mm diameter defect was not able to regenerate up to week 6 without treatment. BL®P was an effective biomaterial for this critical-sized repair and the addition of HG did not compromise bone regeneration. The addition of hDPSC at these specific conditions did not improve outcomes at weeks 3 and 6. As histologically observed, all treatments were free of any adverse reaction to the biomaterials used, providing safety validation of all intervening components: BL®P, HG an hDPSCs. Generally, granules were surrounded by new bone and connective tissue, evidencing the presence of osteoblasts, osteoclasts and vessels, reflecting a good osseointegration and osteoconduction, as previously reported for other Bonelike® granules [14,41]. The mechanism involved in enhancing bone repair is likely correlated with the supply of biologically active ions through BL®P surface (e.g. calcium release), resulting in a favorable microenvironment for apatite formation and osteoid matrix deposition by activated osteoblasts [52]. Indeed, molecular signals (e.g. calcium) are capable of triggering cell differentiation into osteoblastic cell lines, initiating the induction of bone formation as a secondary response [53]. Thus, degradation of calcium-containing BL®P mimics the bone remodeling mechanism, resulting in an osteoinductive microenvironment. At week 3, the presence of the HG formulations, irrespective of cells presence, exhibited a slight apparent delay on bone mineralization compared to BL®P granules, but later converged to much similar values at week 6, being indicative of HG degradation during the first weeks. Despite the higher BL®P dissolution rate observed in vitro in the presence of ODEX, granule degradation was not faster than that of bone formation in vivo, therefore still providing an adequate scaffold.

This work shows evidence that allogenic transplantation of hDPSCs is a safe therapeutic strategy for the repair of bone defects.

This work shows evidence that allogenic transplantation of hDPSCs is a safe therapeutic strategy for the repair of bone defects. There are several studies that over the last few years have demonstrated the ability and tendency of hDPSCs to follow different lines of differentiation when subjected to appropriate in vitro or in vivo stimuli, particularly osteogenic differentiation, which is especially relevant in this work [23,41,47]. In this way, even without a specific immunoselection of the cells used, considering the work previously carried out by our research group and by other researchers regarding the isolation, characterization and demonstration of the capacity for osteogenic differentiation of these cells, the hDPSCs could be used with safety. It is also known that MSCs from different origins express angiogenic markers, have proangiogenic characteristics and the ability to promote endogenous angiogenesis through microenvironmental modulation. This ability sequentially promotes an increase in local vascularization and better tissue regeneration secondary to better nutrition and oxygenation of the tissues under repair. This effect can also be noticed in this work, where an increase in the number of new blood vessels was observed during the histological evaluation, eventually stimulated by the proangiogenic effects of the applied hDPSCs 54,[55].

Although significant improvements on bone deposition could not be perceived. This may be explained by inadequacy of time-points or cell dose, for instance. In another work, a hDPSCs dose of 10^5 cells per 5 mm Ø defect (non-critical) was able to improve bone regeneration in an ovine model after 60 and 120 days, i.e. week 8 and 16. Therefore, a positive effect at later stages should not be excluded in this work, along with different cell dose. Moreover, large animals present large variability between individuals. With a limited number of animals, due to

costs and ethical issues, a single cell dose of 10^6 was tested. Other doses should be addressed, together with different time-points. Yet, preliminary outcomes could be attained, such adding pre-clinical data on safety validation on host tissue-biomaterial interaction and cell transplantation methodology that can help designing future experimental setups. The conditions towards effective stem cell transplantation treatments in critical-sized defects needs more investigation for clinical translation.

5. Conclusion

The addition of HG to BL®P performed comparably to BL®P granules, enabling the regeneration of critical-sized bone defects and, therefore, validating its potential for clinical application as a tool to confer easy handling, injectability and moldability, while simultaneously acting as a carrier of cells for bone regeneration purposes. The HG is an advanced 3D carrier instead of a simple sticky binder. However, the presence of hDPSCs did not accelerate bone formation until week 6, although a positive effect at latter stages or with a different cell dose should not be excluded.

Data availability

No data was used for the research described in the article.

CRediT authorship contribution statement

Alexandra Machado: Formal analysis, Investigation, Methodology, Writing – original draft, Visualization. **Isabel Pereira:** Investigation, Methodology, Supervision, Writing – review & editing. **José Eduardo Pereira:** Conceptualization, Methodology, Resources, Supervision, Writing – review & editing. **Luís Maltez:** Investigation. **Ana Brandão:** Methodology, Resources, Writing – review & editing. **Rui Alvites:** Formal analysis, Methodology, Investigation, Visualization, Writing – original draft. **Ana Catarina Sousa:** Formal analysis, Methodology, Investigation, Visualization, Writing – original draft. **Mariana Branquinho:** Formal analysis, Methodology, Investigation, Visualization, Writing – original draft. **Ana Rita Caseiro:** Formal analysis, Methodology, Investigation, Visualization, Writing – original draft. **Sílvia Santos Pedrosa:** Formal analysis, Methodology, Investigation, Visualization, Writing – original draft. **Ana Colette Maurício:** Conceptualization, Methodology, Resources, Supervision, Writing – review & editing. **Isabel Pires:** Investigation, Validation, Resources. **Justina Prada:** Investigation, Validation, Resources. **José Domingos Santos:** Conceptualization, Methodology, Resources, Supervision, Writing – review & editing. **Miguel Gama:** Conceptualization, Methodology, Resources, Supervision, Writing – review & editing.

Declaration of Competing Interest

The authors declare the following financial interests/personal relationships which may be considered as potential competing interests:

All authors reports financial support was provided by portuguese Fundation for Science and Technology (FCT).

Acknowledgements and funding

Alexandra Machado and Isabel Pereira were supported by the grants SFRH/BD/132000/2017 and UMINHO/BI/131/2018 respectively, from Portuguese Foundation for Science and Technology (FCT), Portugal. The authors acknowledge the funding from FEDER and NORTE 2020 through the project no. 003262 titled “iBONE therapies: advanced solutions for bone regeneration”. This study was supported by FCT under the scope of the strategic funding of UID/BIO/04469 unit and COMPETE 2020 (POCI-01-0145-FEDER-006684) and BioTecNorte operation (NORTE-01-0145-FEDER-000004) funded by the European Regional Development Fund under the scope of Norte 2020 - Programa Operacional Regional do Norte. The participation of Isabel Pires, Justina Prada, Luís Maltez and José Eduardo Pereira was funded by the projects UIDB/CVT/00772/2020 and LA/P/0059/2020 supported by FCT. The participation of Rui Alvites, Ana Catarina Sousa, Mariana Branquinho, Ana Rita Caseiro, Sílvia Santos Pedrosa and Ana Colette Maurício was funded by Projects PEst-OE/AGR/UI0211/2011, UIDB/CVT/00772/2020 and LA/P/0059/2020. Mariana Vieira Branquinho (SFRH/BD/146172/2019) and Ana Catarina Sousa (SFRH/BD/146689/2019) acknowledge FCT, for financial support.

References

[1] E.H. Schemitsch, Size matters: defining critical in bone defect size!, J. Orthop. Trauma 31 (2017) S20–S22, https://doi.org/10.1097/BOT.0000000000000978.
[2] Bone Graft And Substitutes Market Size, Share & Trends Analysis Report By Material Type (Allograft, Synthetic), By Application (Craniomaxillofacial, Dental, Foot & Ankle), By Region, And Segment Forecasts, 2021–2028, Grand View Research, Inc., 2021, p. 145. Report ID: GVR-1-68038-154-2.
[3] C.E. Gillman, A.C. Jayasuriya, FDA-approved bone grafts and bone graft substitute devices in bone regeneration, Mater. Sci. Eng. C 130 (2021), 112466.
[4] World Health Organization. Ageing and health [Internet]. Date Accessed 2022-08-14. https://www.who.int/news-room/fact-sheets/detail/ageing-and-health. 2021.
[5] E. Fiume, G. Magnaterra, A. Rahdar, E. Verné, F Baino, Hydroxyapatite for biomedical applications: a short overview, Ceramics 4 (4) (2021) 542–563, https://doi.org/10.3390/CERAMICS4040039.
[6] F. Duarte, J.D. Santos, A. Afonso, Medical applications of Bonelike® in maxillofacial surgery, Mater. Sci. Forum 455–456 (2004) 370–373, https://doi.org/10.4028/www.scientific.net/MSF.455-456.370.
[7] M. Gutierres, N. Sooraj Hussain, A. Afonso, L. Almeida, T. Cabral, M.A. Lopes, et al., Biological behaviour of Bonelike® graft implanted in the tibia of humans, Key Eng. Mater. 284–286 (2005) 1041–1044, https://doi.org/10.4028/www.scientific.net/KEM.284-286.1041.
[8] M. Gutierres, N.S. Hussain, M.A. Lopes, A. Afonso, A.T. Cabral, L. Almeida, et al., Histological and scanning electron microscopy analyses of bone/implant interface using the novel Bonelike® synthetic bone graft, J. Orthop. Res. 24 (5) (2006) 953–958, https://doi.org/10.1002/jor.20117.
[9] J.V. Lobato, N. Sooraj Hussain, C.M. Botelho, A.C. Maurício, J.M. Lobato, M. A. Lopes, et al., Titanium dental implants coated with Bonelike®: clinical case report, Thin Solid Films 515 (1) (2006) 279–284, https://doi.org/10.1016/j.tsf.2005.12.151.
[10] J.V. Lobato, N.S. Hussain, M.A. Lopes, J.M. Lobato, A.C. Mauricio, A. Afonso, et al., Clinical applications of titanium dental implants coated with glass-reinforced hydroxyapatite composite (Bonelike®), Int. J. Nanomanuf. 2 (1–2) (2008) 135–148, https://doi.org/10.1504/IJNM.2008.017845.
[11] M. Gutierres, A.G. Dias, M.A. Lopes, N.S. Hussain, A.T. Cabral, L. Almeida, et al., Opening wedge high tibial osteotomy using 3D biomodelling Bonelike® macroporous structures: case report, J. Mater. Sci. Mater. Med. 18 (12) (2007) 2377–2382, https://doi.org/10.1007/s10856-007-3171-x.
[12] M. Gutierres, M.A. Lopes, N. Sooraj Hussain, A.F. Lemos, J.M.F. Ferreira, A. Afonso, et al., Bone ingrowth in macroporous Bonelike® for orthopaedic applications, Acta Biomater. 4 (2) (2008) 370–377, https://doi.org/10.1016/j.actbio.2007.06.009.
[13] R.C. Sousa, J.V. Lobato, A.C. Maurício, N.S. Hussain, C.M. Botelho, M.A. Lopes, et al., A clinical report of bone regeneration in maxillofacial surgery using bonelike® synthetic bone graft, J. Biomater. Appl. 22 (4) (2008) 373–385, https://doi.org/10.1177/0885328207078260.
[14] P.O. Pinto, M.V. Branquinho, A.R. Caseiro, A.C. Sousa, A. Brandão, S.S. Pedrosa, et al., The application of Bonelike® Poro as a synthetic bone substitute for the management of critical-sized bone defects—A comparative approach to the autograft technique—A preliminary study, Bone Rep. 14 (2021), 101064, https://doi.org/10.1016/J.BONR.2021.101064.
[15] ISO 13175-3. Implants for surgery—Calcium phosphates—Part 3: hydroxyapatite and beta-tricalcium phosphate bone substitutes. 2012.
[16] N. Abbasi, S. Hamlet, R.M. Love, N.T Nguyen, Porous scaffolds for bone regeneration, J. Sci. Adv. Mater. Devices 5 (1) (2020) 1–9.
[17] G. Iviglia, C. Cassinelli, E. Torre, F. Baino, M. Morra, C Vitale-Brovarone, Novel bioceramic-reinforced hydrogel for alveolar bone regeneration, Acta Biomater. 44 (2016) 97–109, https://doi.org/10.1016/j.actbio.2016.08.012.
[18] A.E. Rodriguez, H. Nowzari, The long-term risks and complications of bovine-derived xenografts: a case series, J. Indian Soc. Periodontol. 23 (5) (2019) 487, https://doi.org/10.4103/JISP.JISP_656_18.
[19] T.Y. Wang, S.L. Xu, Z.P. Wang, J.Y. Guo, Mega-oss and Mega-TCP versus Bio-Oss granules fixed by alginate gel for bone regeneration, BDJ Open 6 (1) (2020) 1–8, https://doi.org/10.1038/s41405-020-0042-8.
[20] M. Kozakiewicz, T. Wach, New oral surgery materials for bone reconstruction—A comparison of five bone substitute materials for dentoalveolar augmentation, Materials (Basel) 13 (13) (2020), https://doi.org/10.3390/MA13132935.
[21] V.R. Patil, A.H. Kharat, D.G. Kulkarni, S.M. Kheur, R.R. Bhonde, Long term explant culture for harvesting homogeneous population of human dental pulp stem cells, Cell Biol. Int. 42 (12) (2018) 1602–1610, https://doi.org/10.1002/CBIN.11065.
[22] M. Kot, M. Baj-Krzyworzeka, R. Szatanek, A. Musiał-Wysocka, M. Suda-Szczurek, M. Majka, The importance of HLA assessment in “off-the-shelf” allogeneic

mesenchymal stem cells based-therapies, Int. J. Mol. Sci. 20 (22) (2019) 5680, https://doi.org/10.3390/IJMS20225680.
[23] S. Awais, S.S. Balouch, N. Riaz, M.S. Choudhery, Human dental pulp stem cells exhibit osteogenic differentiation potential, Open Life Sci. 15 (1) (2020) 229, https://doi.org/10.1515/BIOL-2020-0023.
[24] M. Riccio, E. Resca, T. Maraldi, A. Pisciotta, A. Ferrari, G. Bruzzesi, et al., Human dental pulp stem cells produce mineralized matrix in 2D and 3D cultures, Eur. J. Histochem. 54 (4) (2010) 205–213, https://doi.org/10.4081/EJH.2010.E46.
[25] D.L. Alge, D. Zhou, L.L. Adams, B.K. Wyss, M.D. Shadday, E.J. Woods, et al., Donor-matched comparison of dental pulp stem cells and bone marrow-derived mesenchymal stem cells in a rat model, J. Tissue Eng. Regen Med. 4 (1) (2010) 73–81, https://doi.org/10.1002/TERM.220.
[26] F. Lorusso, F. Inchingolo, G. Dipalma, F. Postiglione, S. Fulle, A. Scarano, Synthetic scaffold/dental pulp stem cell (DPSC) tissue engineering constructs for bone defect treatment: an animal studies literature review, Int. J. Mol. Sci. 21 (24) (2020) 9765, https://doi.org/10.3390/IJMS21249765.
[27] Z. Zhang, Y. Gan, Y. Guo, X. Lu, X. Li, Animal models of vertical bone augmentation (Review), Exp. Ther. Med. 22 (3) (2021) 1–13, https://doi.org/10.3892/ETM.2021.10351.
[28] R.D. Alvites, M.V. Branquinho, A.C. Sousa, B. Lopes, P. Sousa, C. Mendonça, et al., Small ruminants and its use in regenerative medicine: recent works and future perspectives, Biology (Basel) 10 (3) (2021) 249, https://doi.org/10.3390/BIOLOGY10030249.
[29] L.G. Gómez-Mascaraque, J.A. Méndez, M. Fernández-Gutiérrez, B. Vázquez, J. San Román, Oxidized dextrins as alternative crosslinking agents for polysaccharides: application to hydrogels of agarose–chitosan, Acta Biomater. 10 (2) (2014) 798–811, https://doi.org/10.1016/j.actbio.2013.10.003.
[30] S. Li, Y. Xia, Y. Qiu, X. Chen, S Shi, Preparation and property of starch nanoparticles reinforced aldehyde–hydrazide covalently crosslinked PNIPAM hydrogels, J. Appl. Polym. Sci. 135 (5) (2018) 45761, https://doi.org/10.1002/APP.45761.
[31] D. Wang, Y. Xia, D. Zhang, X. Sun, X. Chen, S. Oliver, et al., Hydrogen-bonding reinforced injectable hydrogels: application as a thermo-triggered drug controlled-release system, ACS Appl. Polym. Mater. 2 (4) (2020) 1587–1596, https://doi.org/10.1021/acsapm.9b01232.
[32] P. Bhalla, A.K. Sharma, B.S. Kaith, S. Sehgal, Bhagyashree, S Arora, Synthesis of dextrin-polyacrylamide and boric acid based tough and transparent, self-healing, superabsorbent film, Int. J. Biol. Macromol. 182 (2021) 712–721, https://doi.org/10.1016/J.IJBIOMAC.2021.04.028.
[33] "Food And Drugs." Code of Federal Regulations, title 21 (2021), Chapter I, Subchapter B, Part 184, Subpart B §184.1277.
[34] D.M. Silva, C. Nunes, I. Pereira, A.S.P. Moreira, M.R.M. Domingues, M.A. Coimbra, et al., Structural analysis of dextrins and characterization of dextrin-based biomedical hydrogels, Carbohydr. Polym. 114 (2014) 458–466, https://doi.org/10.1016/j.carbpol.2014.08.009.
[35] D. Hreczuk-Hirst, D. Chicco, L. German, R. Duncan, Dextrins as potential carriers for drug targeting: tailored rates of dextrin degradation by introduction of pendant groups, Int. J. Pharm. 230 (1–2) (2001) 57–66, https://doi.org/10.1016/S0378-5173(01)00859-6.
[36] Y. Kaneo, T. Uemura, T. Tanaka, S. Kanoh, Polysaccharides as drug carriers: biodisposition of fluorescein-labeled dextrans in mice, Biol. Pharm. Bull. 20 (2) (1997) 181–187, https://doi.org/10.1248/BPB.20.181.
[37] Asai T., Kawai T. Bone filling material comprising sintered titanium dioxide and dextrin and method for reconstructing bone defects using the same [Internet]. US20120064172A1, 2010.
[38] M. Molinos, V. Carvalho, D.M. Silva, F.M. Gama, Development of a hybrid dextrin hydrogel encapsulating dextrin nanogel as protein delivery system, Biomacromolecules 13 (2) (2012) 517–527, https://doi.org/10.1021/bm2015834.
[39] Z. Zhang, C. He, X. Chen, Hydrogels based on pH-responsive reversible carbon–nitrogen double-bond linkages for biomedical applications, Mater. Chem. Front. 2 (10) (2018) 1765–1778, https://doi.org/10.1039/C8QM00317C.
[40] D.M. Silva, A.R. Caseiro, I. Amorim, I. Pereira, F. Faria, T. Pereira, et al., Inflammatory response to dextrin-based hydrogel associated with human mesenchymal stem cells, urinary bladder matrix and Bonelike ® granules in rat subcutaneous implants, Biomed. Mater. 11 (6) (2016), 065004, https://doi.org/10.1088/1748-6041/11/6/065004.
[41] I. Pereira, J.E. Pereira, L. Maltez, A. Rodrigues, C. Rodrigues, M. Oliveira, et al., Regeneration of critical-sized defects, in a goat model, using a dextrin-based hydrogel associated with granular synthetic bone substitute, Regen Biomater. 8 (1) (2021) 1–10, https://doi.org/10.1093/rb/rbaa036.
[42] I. Pereira, S. Fraga, L. Maltez, J. Requicha, L. Guardão, J. Oliveira, et al., In vivo systemic toxicity assessment of an oxidized dextrin-based hydrogel and its effectiveness as a carrier and stabilizer of granular synthetic bone substitutes, J. Biomed. Mater. Res. Part A 107 (8) (2019) 1678–1689, https://doi.org/10.1002/jbm.a.36683.
[43] I. Pereira, S. Fraga, S. Silva, J.P. Teixeira, M. Gama, In vitro genotoxicity assessment of an oxidized dextrin-based hydrogel for biomedical applications, J. Appl. Toxicol. 39 (4) (2019) 639–649, https://doi.org/10.1002/jat.3754.
[44] J.M. Campos, A.C. Sousa, A.R. Caseiro, S.S. Pedrosa, P.O. Pinto, M.V. Branquinho, et al., Dental pulp stem cells and Bonelike® for bone regeneration in ovine model, Regen Biomater. 6 (1) (2019) 49–59, https://doi.org/10.1093/rb/rby025.
[45] J. Torres, M. Gutierres, L. Atayde, P. Cortez, M.A. Lopes, J.D. Santos, et al., The benefit of bone marrow concentrate in addition to a glass-reinforced hydroxyapatite for bone regeneration: an in vivo ovine study, J. Orthop. Res. 35 (6) (2017) 1176–1182, https://doi.org/10.1002/JOR.22800.
[46] L.M. Atayde, P.P. Cortez, A. Afonso, M. Santos, A.C. Maurício, J.D. Santos, Morphology effect of bioglass-reinforced hydroxyapatite (Bonelike ®) on osteoregeneration, J. Biomed. Mate.r Res. Part B Appl. Biomater. 103 (2) (2015) 292–304, https://doi.org/10.1002/jbm.b.33195.
[47] A.R. Caseiro, S. Santos Pedrosa, G. Ivanova, M. Vieira Branquinho, A. Almeida, F. Faria, et al., Mesenchymal stem/stromal cells metabolomic and bioactive factors profiles: a comparative analysis on the umbilical cord and dental pulp derived stem/ stromal cells secretome, Papaccio G, editor, PLoS One 14 (11) (2019), e0221378, https://doi.org/10.1371/journal.pone.0221378.
[48] K. Ishikawa, Y. Miyamoto, A. Tsuchiya, K. Hayashi, K. Tsuru, G. Ohe, Physical and histological comparison of hydroxyapatite, carbonate apatite, and β-tricalcium phosphate bone substitutes, Materials (Basel) 11 (10) (2018) 1993, https://doi.org/10.3390/MA11101993.
[49] Y. Liu, Z. Li, J. Li, S. Yang, Y. Zhang, B. Yao, et al., Stiffness-mediated mesenchymal stem cell fate decision in 3D-bioprinted hydrogels, Burn trauma 8 (2020) tkaa029, https://doi.org/10.1093/BURNST/TKAA029.
[50] J. Xu, M. Sun, Y. Tan, H. Wang, H. Wang, P. Li, et al., Effect of matrix stiffness on the proliferation and differentiation of umbilical cord mesenchymal stem cells, Differentiation 96 (2017) 30–39, https://doi.org/10.1016/J.DIFF.2017.07.001.
[51] F.R. Maia, K.B. Fonseca, G. Rodrigues, P.L. Granja, C.C. Barrias, Matrix-driven formation of mesenchymal stem cell-extracellular matrix microtissues on soft alginate hydrogels, Acta Biomater. 10 (7) (2014) 3197–3208, https://doi.org/10.1016/J.ACTBIO.2014.02.049.
[52] M.G. Gandolfi, G. Iezzi, A. Piattelli, C. Prati, A. Scarano, Osteoinductive potential and bone-bonding ability of ProRoot MTA, MTA plus and biodentine in rabbit intramedullary model: microchemical characterization and histological analysis, Den.t Mater. 33 (5) (2017) e221–e238, https://doi.org/10.1016/J.DENTAL.2017.01.017.
[53] U. Ripamonti, Biomimetism, biomimetic matrices and the induction of bone formation, J. Cell Mol. Med. 13 (9 B) (2009) 2953–2972.
[54] S.M. Watt, F. Gullo, M. Van Der Garde, D. Markeson, R. Camicia, C.P. Khoo, et al., The angiogenic properties of mesenchymal stem/stromal cells and their therapeutic potential, Br. Med. Bull. 108 (1) (2013) 25–53, https://doi.org/10.1093/BMB/LDT031.
[55] H. Tao, Z. Han, Z.C. Han, Z. Li, Proangiogenic features of mesenchymal stem cells and their therapeutic applications, Stem Cells Int. 2016 (2016) 11, https://doi.org/10.1155/2016/1314709. , 1314709.